DZero H-Disk Cooling Channel Fluid / Thermal Design

Greg Derylo
March 30, 1998

1.0 Introduction

Each H-disk ring assembly is comprised of 24 wedge assemblies that are mounted to a ring that provides both structural support and cooling to the detector wedges. Figure 1-1 shows the general layout of a disk assembly.

In order for the H-disks to operate on the same cooling system as the rest of the silicon detectors, the pressure drop must be compatible with that of the overall system design. That is, the pressure drop for which the system is to operate, which will include cooling channels for bulkheads, F-disks, and H-disks, should yield unthrottled flowrates in each cooling device that result in acceptable fluid temperature rises due to their respective heat loads[1]. Too low a pressure drop in any channel would either rob flow from other portions of the detector or require that a higher total flowrate be supplied by the cooling system. Too high a pressure drop would yield an unacceptably large fluid temperature rise across the H-disk ring.

In order to keep the detector temperatures low, thus reducing the effect of radiation damage to the silicon, the channel design should also minimize the difference between the bulk fluid temperature and the temperature of the mounting surfaces to which the wedges are attached. This is a significant portion of the overall temperature difference between the coolant fluid and the hottest portion of the silicon.

This report compares calculated pressure drops to test results measured on ring mock-ups for two different channel designs. The cross-section of the two different channels discussed here are shown in Figure 1-2. Channel A is a simple rectangle with a 1 x 16 mm cross section, while Channel B has a serpentine cross section but maintains a width of 1 mm.

Channel A represents an early design concept while Channel B represents the culmination of the design evolution. The serpentine Channel B design has a larger cross-sectional area than Channel A (29 vs. 16 square mm), so it is expected to have a lower ΔP. Its larger surface area, while maintaining the same gap height, provides improved heat transfer performance. Both of these channels assume that the ring inlet and outlet are 180° apart with the flow evenly split between ring halves. Channel configurations that had a single 360° channel were also considered. However, in order to keep ΔPs low, larger channels were required to accommodate the higher flows through the channel, and larger gap heights lead to larger fluid-to-wall temperature differences. Therefore, this option was not developed further.

[1] Although throttling could potentially be used for flow balancing, it has been decided that no throttling will be used due to long-term stability concerns.

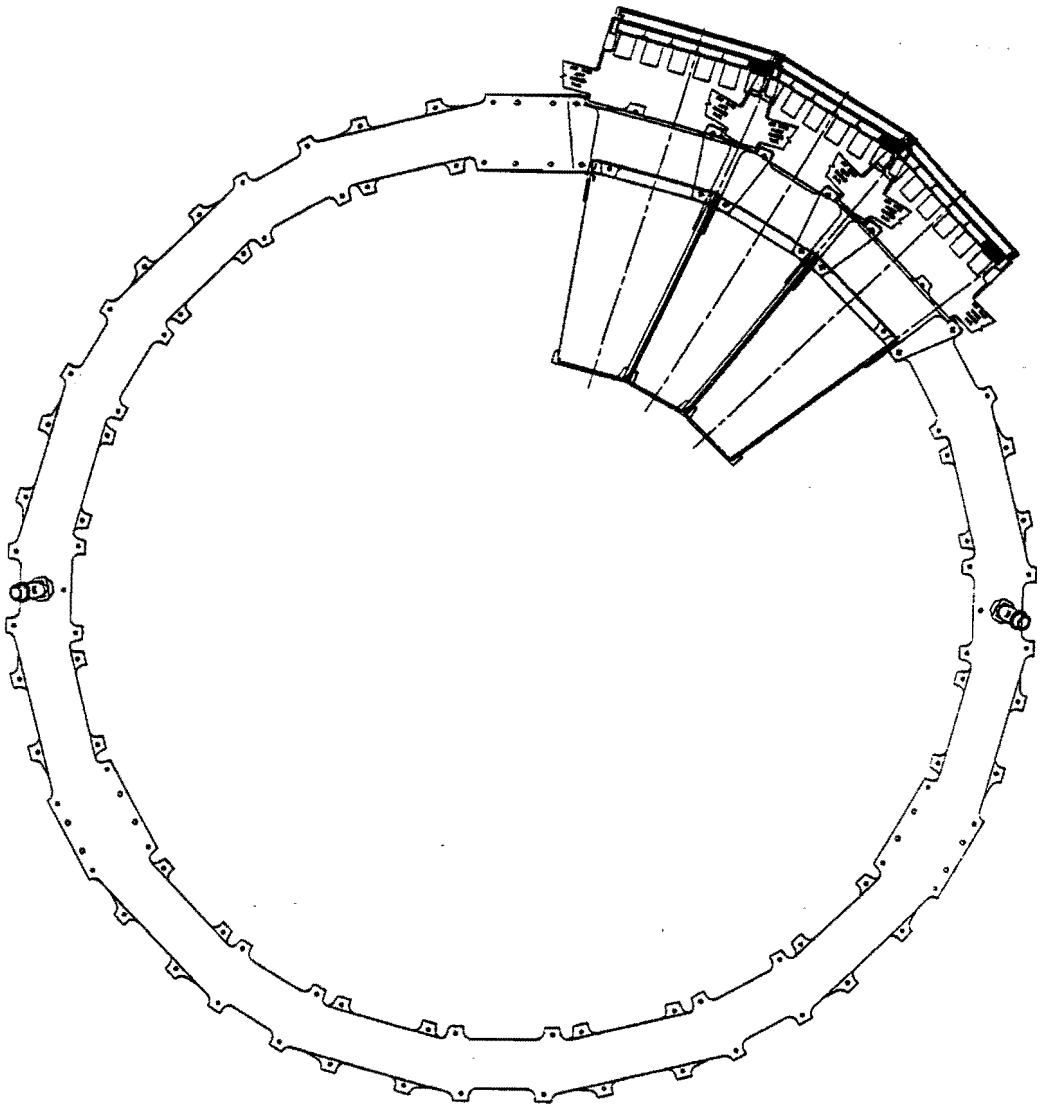

Figure 1-1: H-Disk Cooling Ring

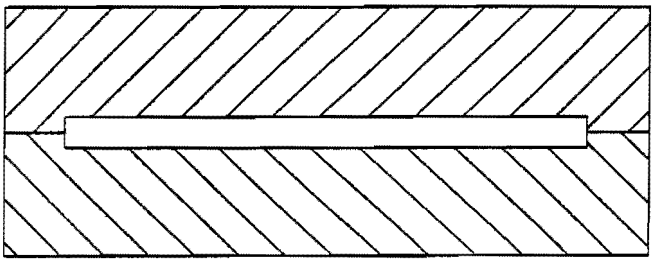

Channel A Cross Section

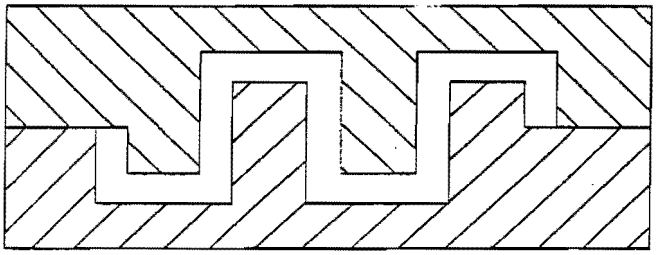

Channel B Cross Section

Figure 1-2: Channels A & B Cross Sections

2.0 Analysis

2.1 Pressure Drop Predictions and Test Results

A pressure drop model was first developed for the H-disk ring in order to evaluate various cooling channel designs. The following system conditions were assumed:

a. Coolant is 30% ethylene glycol by weight in water.

b. Coolant temperatures of -10 and 0 °C are studied.

c. H-Disk nominal heat load is based on an SVX II chip heat load of 0.64 Watts [1]. For 24 wedges, each with 12 chips, this results in a total heat load of 184.32 Watts. Additional (convective) heat loads [5] are not considered here.

d. In order to establish a convenient flowrate value for comparison to the bulkhead and F-disk cooling channels, a reference flowrate is determined at which the nominal heat load yields a 1°C coolant temperature rise. Nominal flowrates vs. effective coolant temperature are shown below:

Effective Coolant Temperature (°C)	Reference Flowrate (lpm)
-10	2.929
0	2.915
+10	2.901

The friction factor for fully developed laminar flow in rectangular channels was calculated using the data in Reference 2 Chapter 7 Table 33, which gives ($f_{Fanning}$ * Re) as a function of rectangular aspect ratio. Reynolds number values calculated for the various cases were very low, as shown in Tables 2.1-1 and 2.1-2, such that laminar flow was the applicable flow regime for all cases (Re_{crit} ~ 2500 [2]). Calculated entry length indicator values ($L/D_h/Re$) demonstrated that the flow could be treated as fully developed rather than developing laminar flow. Based on benchmarking done to F-disk channel mock-up data, the channel length (L) used for this entry length calculation used the full 180° path length (588 mm assumed) rather than a 15° path segment since the corner bends apparently have a minimal effect on flow mixing. Also, based on this F-disk benchmarking, no additional pressure drop factors were included to account for corner bends or inlet/outlet losses.

The Channel B design, with its serpentine cross-section, does not lend itself directly to use of the rectangular channel correlation. However, as a first approximation, this correlation is used on this design by treating it as a very wide rectangular channel, effectively stretching it out such that the gap height and total surface area are maintained. This creates a channel size of 1 x 29 mm for this design.

The calculated pressure drops for Channel A and B are shown in Tables 2.1-1 and 2.1-2, respectively. As expected, Channel B has a lower pressure drop due to its larger cross-sectional area. As mentioned above, the Reynolds number values are quite low.

Table 2.1-1: Channel A (1 x 16 mm) ΔP Predictions

Flowrate (FON)	Tavg = -10°C		Tavg = 0°C	
	Re (---)	ΔP (psi)	Re (---)	ΔP (psi)
1.4	681	14.1	1086	8.7
1.3	632	13.1	1008	8.1
1.2	583	12.1	931	7.5
1.1	353	11.1	853	6.8
1.0	486	10.1	776	6.2
0.9	438	9.1	698	5.6
0.8	389	8.0	620	5.0
0.7	340	7.0	543	4.4
0.6	292	6.0	465	3.7
0.5	243	5.0	388	3.1
0.4	194	4.0	310	2.5
0.3	146	3.0	233	1.9
0.2	97	2.0	155	1.2

Table 2.1-2: Channel B (1 x 29 mm) ΔP Predictions

Flowrate (FON)	Tavg = -10°C		Tavg = 0°C	
	Re (---)	ΔP (psi)	Re (---)	ΔP (psi)
1.4	386	9.7	615	4.7
1.3	358	8.8	571	4.4
1.2	331	8.0	527	4.0
1.1	303	7.1	483	3.7
1.0	275	6.4	440	3.4
0.9	248	5.9	396	3.0
0.8	220	5.3	352	2.7
0.7	193	4.6	308	2.4
0.6	165	3.8	264	2.0
0.5	138	2.9	220	1.7
0.4	110	2.2	176	1.3
0.3	83	1.7	132	1.0
0.2	55	1.1	88	0.7

Plexiglas mock-ups of Channels A and B were fabricated and were found to be accurate to within a few mils. They were then tested with the coolant system stand constructed at the Fermilab Proton Assembly Building. Flow measurement was performed with two Gilmont float-type flowmeters with different flow capacities placed in parallel (only one was used at a time). Pressure drop measurement was performed via a Sensotec differential pressure transmitter with taps located approximately four inches from the ring nozzles. Temperature measurement was achieved with RTDs located directly in the coolant near the ring inlet and outlet (outboard of the pressure taps) and near the flowmeters. Pressure drop behavior was measured at -10, 0, and +10 °C.

Figure 2.1-1 shows the Channel A (1 x 16 mm channel) test data as well as predicted pressure drops. Due to the rapid increase in coolant viscosity as the freezing point (approximately -14.6°C) is approached, the pressure drop is much higher at -10°C than it is at warmer temperatures. At -10°C, the correlation between predicted and actual pressure drops is excellent. At 0°C, the match is very good at low flowrates, but much less so at higher flows. It should be noted that the jump in the measured data curve occurs at the point at which the transition is made between the high flow and low flow flowmeters.

At -10°C, a flowrate which yields a 1°C coolant temperature rise across the ring would result in about a 10 psi pressure drop while a lower flowrate yielding a 2°C rise would result in about a 5 psi drop. This linearity is consistent with expected laminar flow pressure drop behavior.

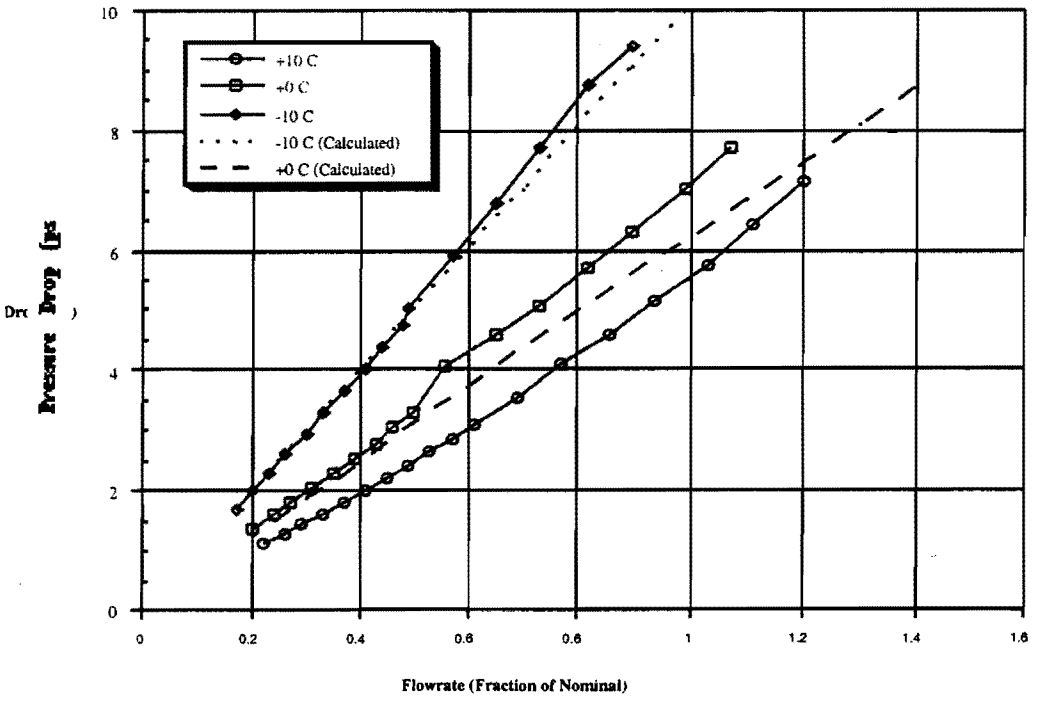

Figure 2.1-1
Channel A (1 x 16 mm) Pressure Drops

Figure 2.1-2 shows the test data and predicted ΔP curves for the Channel B serpentine design. Due to the larger cross-section area, the pressure drop is smaller than that of Channel A. At -10°C, the correlation between predicted and actual pressure drops is excellent at lower flows, but diverges at just below a flow of 0.5 nominal. The simple model developed for this channel therefore does not fully account for the flow behavior of this complicated design.

The same divergence applies for the 0°C prediction, which matches well at low flows but underpredicts the pressure drop at higher flows.

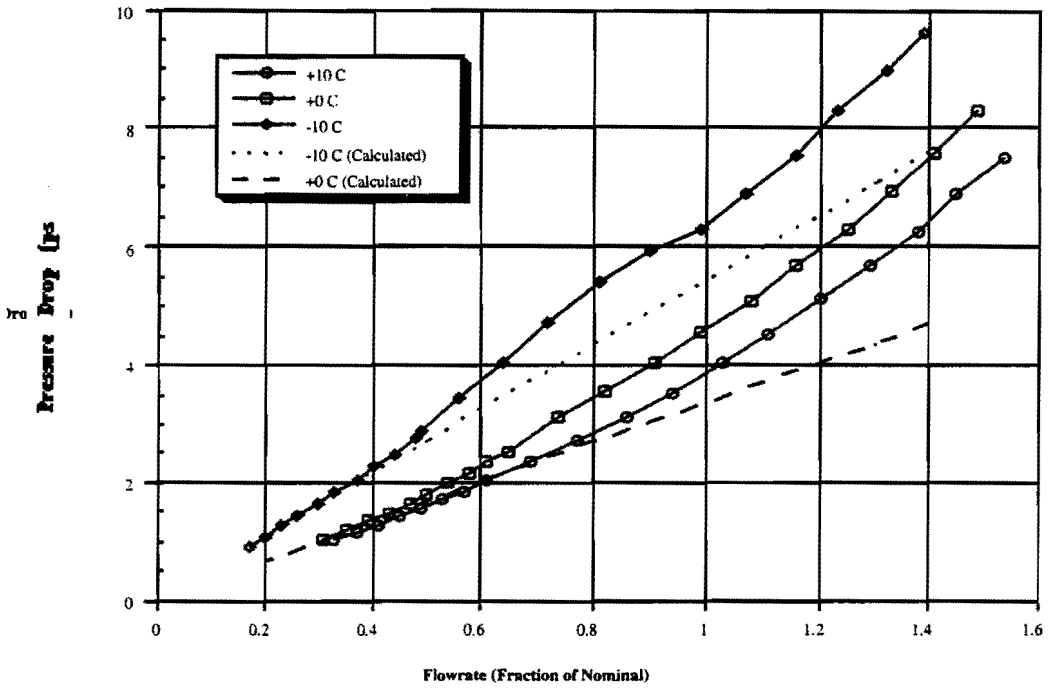

Figure 2.1-2
Channel B (Serpentine Design) Pressure Drops

A comparison of how this data correlates to the performance of a module bulkhead and an F-disk cooling ring can be seen in Figure 2.1-3 below. This plot shows the Channel A and B pressure drop curves at -10°C compared to the other two detector channels [3]. For each channel type, nominal flow is defined as that which yields a 1°C coolant temperature rise for the stated heat load.

The figure shows that the H-disk Channel A curve has the highest pressure drop response. The H-disk Channel B design provides a lower bound to the bulkhead and F-disk channels and is a much closer match to the other detector channel types than Channel A.

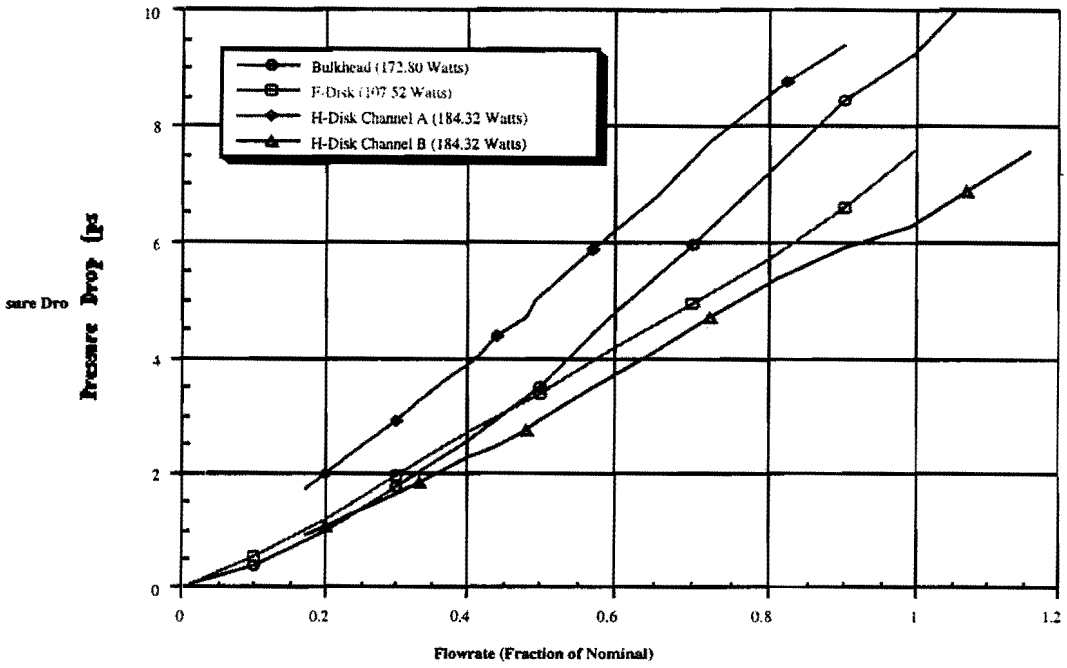

Figure 2.1-3
H-Disk ΔP Comparison with Bulkhead & F-Disk at -10°C

2.2 Heat Transfer Estimates

As discussed in the Introduction above, the effectiveness of the cooling channel heat transfer is very important to the overall ring design. In order to keep the detector silicon as cool as possible, unnecessary temperature differences between the coolant and the hottest portion of the silicon should be avoided.

As shown above, the coolant flow is laminar, therefore the coolant essentially flows in smooth streamlines along the channel without the transverse velocity components which mix the flow and which make turbulent flow a much more effective heat transfer mechanism. Without this mode of mixing in the channel, laminar convection heat transfer is relatively poor, with the conduction of heat through the fluid (as opposed to convection) being a significant factor in the performance of the system. Improving the heat transfer is the primary reason for the difference between the two channel designs. The simple 1 x 16 mm Channel A cross section maintains a thin gap height, thus minimizing the fluid thickness through which the heat must conduct when transferring from the ring walls into the coolant. The Channel B design also maintains a thin gap for the same reason,

but the serpentine shape acts to increase the surface area in contact with the coolant, thus reducing the local heat flux. Although designs had been proposed with a greater surface area by increasing the number of fins in the channel (three fins per side rather than the two shown in Figure 1-1) and by adding a narrow milling cut to make the fins at each end full height, they were not pursued due to concerns about relatively thin metal thicknesses and more costly machining steps.

Predictions of the heat transfer performance are based on the information on laminar flow in rectangular ducts included in Reference 2 Chapter 7. This approach first looks at the system thermal entry length to determine whether or not the system can be considered to be fully thermally developed. The axial variable length x^+ is defined as:

$$x^+ = 2 (L / D_h) / (Re * Pr)$$

Consistent with the pressure drop modeling above, the path length used is based on a 180° rather than 15° path, therefore assuming that the bends do not contribute to thermal mixing in the coolant. Calculation of this value indicates that correlations for developing laminar flow are appropriate. The steps then used to estimate the appropriate average Nusselt number were as follows:

- A base Nu_{avg} was estimated for a specific x^+ by integrating Nu_x data for a constant heat flux in rectangular tubes assuming a 1-to-4 aspect ratio
- Nu_{avg} was then adjusted to account for different aspect ratios and to account for the effect of unheated walls
- Convection coefficients were then calculated and used to estimate fluid-to-wall temperature differences given the known heat load and an assumed length over which that heat is assumed to be transferred (66 mm, which roughly corresponds to the size of the wedge substrate region in contact with the ring). For the Channel B design, reduced effectiveness of the surfaces associated with the channel fins was accounted for [4].

The unheated wall issue mentioned in the second item warrants further discussion. The wedge layout in the cooling channel is such that the heat load is applied on alternating sides along the channel. However, the circumferential overlap between adjacent wedges is significant such that approximately 50% of the channel is loaded from both sides of the ring. For the remainder of the ring, heat is applied to only one side. This type of loading results in lower effective convection coefficients. With heat applied through only one channel wall, the fluid thickness through which the which the heat must conduct is increased (essentially the full channel gap height vs. one-half the gap height for an evenly-loaded channel), and as discussed above, this thermal resistance is an important factor in laminar convection heat transfer. Reference 2 Chapter 7 Table 37 shows the Nusselt number behavior for different heated wall arrangements as a function of rectangular aspect ratio.

Some heat, however, is conducted in the ring walls to the back half of the channel. Heat can reach this region via conduction from the heated side of the cooling channel (although the adhesive layer, which has a thermal conductivity two orders of magnitude lower than that of beryllium, creates a large thermal resistance) and from the neighboring wedges which are on the same side of the cooling channel. In an attempt to better understand this behavior, a three-dimensional finite difference conduction model of a Channel B ring section was developed. Unfortunately, the analysis code used for this modeling effort, EES [6], was unable to handle the large number of

nodes needed to model this problem adequately. However, computational results with a course nodalization do show behavior that is consistent with the anticipated trends. This study showed that the channel was evenly loaded in the region with the heat load applied to both sides of the channel. Where the heat load was applied only from one side, the heated side of the channel was found to transfer 2.0 times the rate of the unheated side. A simplification of the model, which only looks at a two-dimensional slice across the cooling channel, showed that the heat transferred on the loaded side was 3.5 times the rate from the unheated side. Since a two-dimensional model does not account for heat transferred along the length of the channel, all the heat transferred from the unheated side of the channel comes from the heated side, through the adhesive layer at the ring midplane. These results indicate that the back side of the unheated channel regions do contribute to the overall removal of heat from both the wedge on the opposite side of the channel and from the neighboring wedges which are on the same side of the channel.

As a simplification, however, the measure of the cooling channel effectiveness used in evaluating cooling ring design performance will not account for this benefit. The coolant-to-wall temperature differences reported here are based on the region in which the channel is heated from both sides with no benefit from heat spreading in the direction along the cooling channel. This yields the largest temperature difference expected for this system. Table 2.2-1 shows the average Nusselt number and fluid-to-wall temperature difference calculated for both the Channel A and Channel B designs for this heat load condition. Only operation at -10°C is included here since the coolant conductivity and specific heat are not largely sensitive to temperature over the temperature range of interest. The same temperature differences are shown graphically in Figure 2.2-1. As expected, the serpentine Channel B design performs notably better than the Channel A design. For 1 and 2°C temperature rises across the ring, the Channel B temperature differences are 32 and 35 percent lower than the Channel A design, respectfully.

Table 2.2-1
Predicted Fluid-to-Wall Heat Transfer for Dual-Sided Heat Loads and -10°C Coolant

	Channel A		Channel B	
Flowrate (FON)	**Nu_{avg}**	**Fluid-to-Wall ΔT (C)**	**Nu_{avg}**	**Fluid-to-Wall ΔT (C)**
1.4	15.7	1.94	14.1	1.34
1.3	15.3	1.99	13.7	1.37
1.2	14.9	2.05	13.3	1.41
1.1	14.5	2.10	13.0	1.44
1.0	14.0	2.17	12.6	1.48
0.9	13.6	2.25	12.1	1.54
0.8	13.0	2.34	11.6	1.60
0.7	12.5	2.45	11.1	1.67
0.6	11.9	2.56	10.6	1.75
0.5	11.1	2.74	10.4	1.78
0.4	10.3	2.95	10.1	1.84
0.3	9.8	3.12	9.7	1.91
0.2	9.2	3.30	9.0	2.05

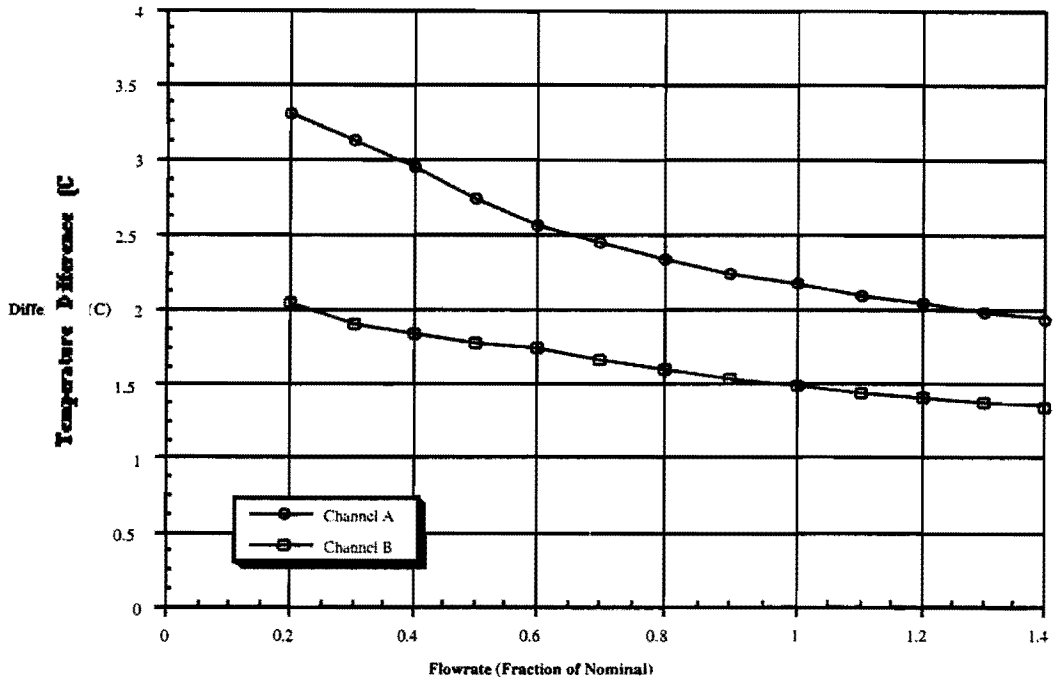

Figure 2.2-1: Fluid-to-Wall Temperature Difference with a Heat Load Applied to Both Ring Faces (operation at -10°C)

Figures 2.2-2and 2.2-3 are shown to illustrate the calculated fluid-to-metal temperature difference correlation to the measured ΔP results for both Channel A and Channel B. Note that these temperature values include an additional resistance contribution resulting from a 1 mil thick low-conductivity primer coating on the interior surface of the cooling channel. The solid lines represent the calculated local temperature differences while the dotted lines include this difference plus the coolant temperature rise across the ring associated with the nominal heat load addition (i.e., 1°C effect at nominal flow). These figures therefore represent the maximum local and overall calculated fluid-to-metal temperature differences as a function of the available cooling system ΔP. For example, for operation at -10°C with a 5 psi pressure drop, the Channel B design can be seen to have local and maximum fluid-to-metal temperature differences 41 and 39 percent lower than Channel A, respectively.

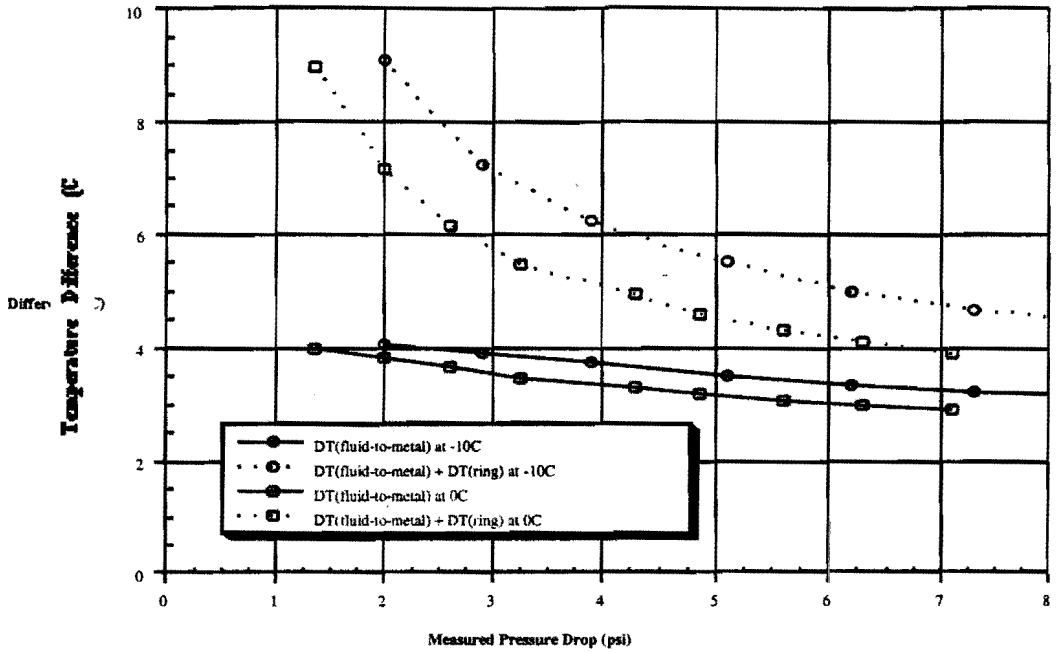

Figure 2.2-2: Channel A Fluid-to-Metal Temperature Difference vs. ΔP with a Heat Load Applied to Both Ring Faces (operation at -10°C)

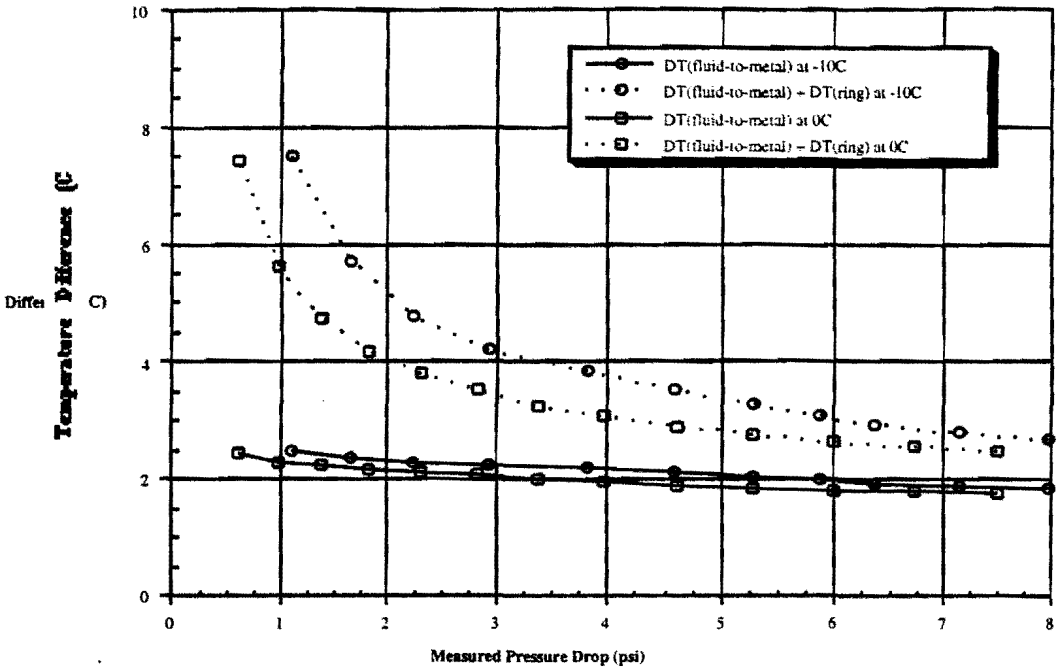

Figure 2.2-3: Channel B Fluid-to-Metal Temperature Difference vs. ΔP with a Heat Load Applied to Both Ring Faces (operation at -10˚C)

3.0 Summary / Conclusions

Based on mock-up testing, the Channel B coolant passage design has a ΔP characteristic consistent with that previously measured for the bulkhead and F-disk cooling channel designs. Channel A was found to have a higher pressure drop. Due to the complicated Channel B shape, analytical modeling was only partially successful at predicting this response. The simpler Channel A design was predicted much more accurately analytically.

Channel B significantly outperforms the Channel A design in terms of the calculated fluid-to-metal temperature differences. For the serpentine Channel B design, local fluid-to-metal ΔTs are estimated to be about 2°C over a wide range in coolant ΔP. In order to confirm the results of these heat transfer estimates, it is recommended that testing be performed on a suitable physical mock-up of the Channel B cooling ring design.

4.0 References

1. Email Message, "Re: NWA Test," from Bill Cooper to Bruce Squires, 2/15/97.

2. Rohsenow, W.E., Hartnett, J.P., and Ganic, E.N., eds., "Handbook of Heat Transfer Fundamentals," 2nd ed., McGraw-Hill Book Co., New York, 1985.

3. Bulkhead and F-disk data from a plot dated 1/19/98 as part of work in progress by Bruce Squires.

4. Incropera, F.P., and DeWitt, D.P., "Fundamentals of Heat and Mass Transfer," 2nd ed., John Wiley & Sons, New York, 1985.

5. Derylo, Greg, "Thermal Analysis of a DZero H-Disk Wedge," D0EN 3823.112-EN-488, 3/30/98.

6. Engineering Equation Solver (EES) version 4.401, by F-Chart Software, Middleton, Wisconsin.